THE JOURNAL OF PHYSICAL CHEMISTRY LETTERS
A JOURNAL OF THE AMERICAN CHEMICAL SOCIETY

pubs.acs.org/JPCL

Letter

Nanoscale Encapsulation of Hybrid Perovskites Using Hybrid Atomic Layer Deposition

Jue Gong, Moein Adnani, Brendon T. Jones, Yan Xin, Sisi Wang, Sawankumar V. Patel, Eric Lochner, Hedi Mattoussi, Yan-Yan Hu, and Hanwei Gao*

Cite This: J. Phys. Chem. Lett. 2022, 13, 4082−4089

Read Online

ACCESS | Metrics & More | Article Recommendations | Supporting Information

ABSTRACT: Organic−inorganic hybrid perovskites have shown tremendous potential for optoelectronic applications. Ion migration within the crystal and across heterointerfaces, however, imposed severe problems with material degradation and performance loss in devices. Encapsulating hybrid perovskite with a thin physical barrier can be essential for suppressing the undesirable interfacial reactions without inhibiting the desirable transport of charge carriers. Here, we demonstrated that nanoscale, pinhole-free Al_2O_3 layer can be coated directly on the perovskite $CH_3NH_3PbI_3$ using atomic layer deposition (ALD). The success can be attributed to a multitude of strategies including surface molecular modification and hybrid ALD processing combining the thermal and plasma-enhanced modes. The Al_2O_3 films provided remarkable protection to the underlying perovskite films, surviving by hours in solvents without noticeable decays in either structural or optical properties. The results advanced the understanding of applying ALD directly on hybrid perovskite and provided new opportunities to implement stable and high-performance devices based on the perovskites.

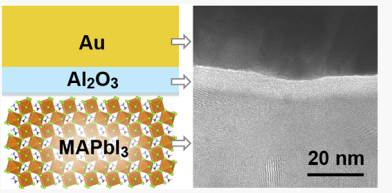

Organic−inorganic hybrid perovskites have shown high performance in optoelectronic devices such as solar cells,[1,2] light and radiation detectors,[3,4] light-emitting diodes, and lasers.[5,6] The remarkable performance stemmed primarily from the pronounced photoresponse (in both optical absorption and emission)[7,8] and efficient charge transport.[9,10] While the functionalities have been demonstrated successfully in research laboratories, development of viable devices remains challenging. Most of the devices showed rapid performance losses under continuous operation.

Among the factors that are responsible for the observed instability, ion migration is particularly difficult to suppress. It has been shown, both theoretically and experimentally, that ions in the hybrid perovskites are inherently mobile due to the soft nature of the crystal lattices and could be further active under external stresses such as moisture (chemical), illumination (optical), or electrical biases.[11−14] The resulted degradation can be twofold: in the bulk of the perovskites, the collective motion of ions could leave behind aggregates of vacancies, which disrupt the integrity of crystal lattices;[15] at heterointerfaces, on the other hand, ions in the perovskites can migrate and react with neighboring layers, or vice versa.[16] Many efforts have been made to address the former problem,[17−19] leaving the latter largely overlooked in previous research.

A potential approach to inhibit the cross-interface ion migration and suppress the interfacial reactions was to passivate the interface with a layer of inert material. This interlayer ought to be chemically impermeable with complete surface coverage and, in the meantime, sufficiently thin to avoid large impedance of charge carrier transport for optoelectronic functionalities. Atomic layer deposition (ALD) could meet all of these criteria and therefore be particularly suitable for implementing such interlayers. By assembling materials in a layer-by-layer fashion at the atomic scale, ALD was known for creating conformal, pinhole-free thin films with atomic precision in thickness.[20]

Conducting ALD directly on the hybrid perovskites was nontrivial. The vulnerable surface chemistry made the perovskites highly sensitive to conditions commonly used in ALD processes, such as water exposure and elevated temperature. Although some attempts have been made to show the potentially desirable effects of ALD interlayers in perovskite-based devices,[21−25] results by different investigations appeared to be inconsistent in terms of the processing conditions, coating quality, and level of damages to the underlying perovskites.[26−29] In this work, we established a hybrid ALD protocol that can be used to coat Al_2O_3 films directly on methylammonium lead iodide ($CH_3NH_3PbI_3$ or $MAPbI_3$ for short), a specific type of hybrid perovskite commonly incorporated in solar cells with great success.[30] Combining the thermal and plasma-enhanced modes, the hybrid ALD produced ultrathin coating with excellent morphological quality, coating efficacy, and chemical compat-

Received: March 24, 2022
Accepted: April 28, 2022

https://doi.org/10.1021/acs.jpclett.2c00862
J. Phys. Chem. Lett. 2022, 13, 4082−4089

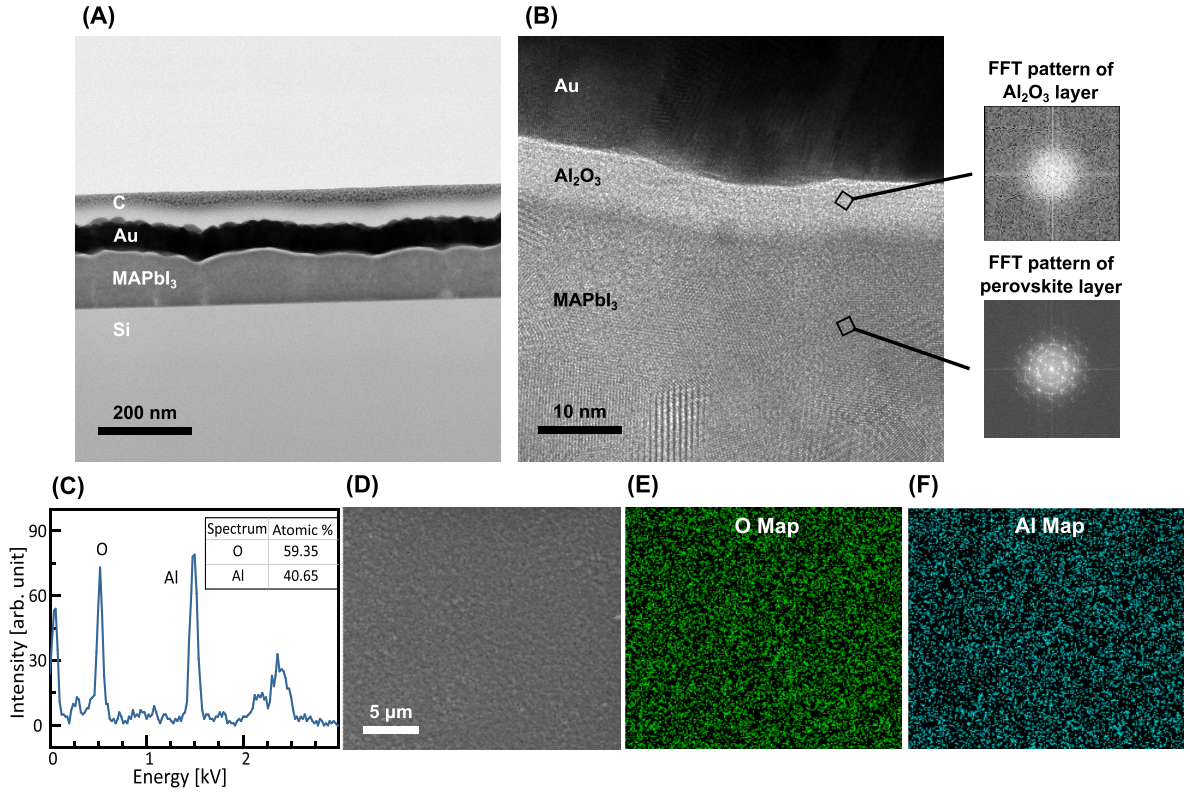

Figure 1. Successful demonstration of ALD-coated Al_2O_3 directly on the perovskite $MAPbI_3$. (A) Cross-section TEM image of surface-treated $MAPbI_3$ coated with 100 cycles of thermal ALD at 90 °C. Layers of carbon and platinum, in addition to a 60 nm thick layer of gold, were sequentially deposited on top of the ALD layer to protect the samples from beam damage during focused ion beam milling. (B) Magnified view of the TEM image. Inset: FFT pattern of the Al_2O_3 and perovskite layer. (C) EDS spectrum of cross-section ALD Al_2O_3 layer shown in (A). (D) Plane-view SEM image of 100 cycles of thermal ALD-coated $MAPbI_3$ and the corresponding EDS mapping of oxygen (E) and aluminum (F).

ibility. Modifying the surface of the perovskite by using selected small molecules was found helpful in preparing the surface for ALD. While bare perovskite films could be dissolved by ethanol within minutes, 7 nm of ALD-coated Al_2O_3 was sufficient to protect the underlying perovskite against the solvent for hours. The remarkable chemical resistance achieved in this work will provide a new path toward stable optoelectronic devices based on hybrid perovskites.

ALD reached atomic-layer precision by delivering alternating precursors in a self-limiting manner.[31] When reaction conditions (e.g., temperature, pressure, and duration) were properly controlled, atomic layers of materials with a desirable composition could be coated in a layer-by-layer fashion, producing a conformal and pinhole-free surface coverage. Al_2O_3 was used in this work as the model material to demonstrate the capability of applying ALD directly on the hybrid perovskites. The inert chemistry of Al_2O_3 was desirable for interfacial stabilization. Following a widely used ALD protocol,[32] we used trimethylaluminum (TMA) as the source of Al and H_2O as the coreactant for oxidation (more details in the Experimental Methods section).

A thin, conformal layer of Al_2O_3 was created successfully on solution-synthesized $MAPbI_3$ (Figure 1). To prepare the surface for ALD reactions, the perovskite was surface-treated by using 2-mercaptoethanol ($HOCH_2CH_2SH$ or 2-mcpEtOH) prior to the ALD processing (more details in Figure 4). Shown in the cross-section transmission electron microscopy (TEM) images, about 7 nm thick Al_2O_3 film was obtained after 100 cycles of ALD (Figure 1A,B).

The coating appeared to be highly uniform in thickness, following the surface contour of the microcrystalline perovskite grains without any noticeable discontinuity (i.e., pinhole-free). The fast Fourier transform (FFT) pattern of the TEM image showed that the Al_2O_3 layer was amorphous (Figure 1B, insets), consistent with the typical crystallinity reported in other ALD-coated Al_2O_3.[32−35] The atomic ratio between Al and O, indicated in the energy-dispersive X-ray spectrum (EDS, Figure 1C), appeared to be close to the 2:3. This ratio matched with the expected stoichiometry of Al_2O_3, implying that the precursors were sufficiently reacted under the chosen conditions. The uniformity of the Al_2O_3 coating was evident at a larger scale in the top-view EDS mapping obtained by using a scanning electron microscope (SEM). Microcrystalline morphology of the perovskite layer could be visualized in the secondary electron image (Figure 1D), whereas the EDS mapping showed a homogeneous distribution of Al and O across the field of view (Figure 1E,F) with the atomic ratio, again, close to 2:3 (Figure S1). A cross-section elemental mapping of $MAPbI_3$ film with 100 cycles of thermal ALD AL_2O_3 is also presented in Figure S2.

A finely tuned substrate temperature was found to be critical to the success of conducting ALD directly on $MAPbI_3$. Hybrid perovskites, because of the organic constituent, were known to be thermally vulnerable. $MAPbI_3$, for example, was reported to decompose above 250 °C under ambient pressure,[36,37] which could occur at a lower temperature in a vacuum. On the other hand, the conventional ALD, also known as thermal ALD, facilitated reactions between precursors and coreactants by elevating the substrate temperature.[33,38,39] Although some

https://doi.org/10.1021/acs.jpclett.2c00862
J. Phys. Chem. Lett. 2022, 13, 4082−4089

materials (e.g., Al_2O_3) could be deposited at a moderate or even room temperature, the low-temperature processing often came at a cost of compromised coating quality mainly due to insufficient precursor reaction or condensation.[40] By sweeping the processing temperature while monitoring the physical properties of the perovskite films, we identified ~120−150 °C to be the highest temperature below which the integrity of $MAPbI_3$ can be retained confidently (Figure 2). Above that window, the PbI_2 phase appeared in the X-ray diffraction (XRD) patterns, indicating that thermal decomposition occurred following a typical reaction $MAPbI_3 \rightarrow PbI_2 + CH_3I + NH_3$.[41−43]

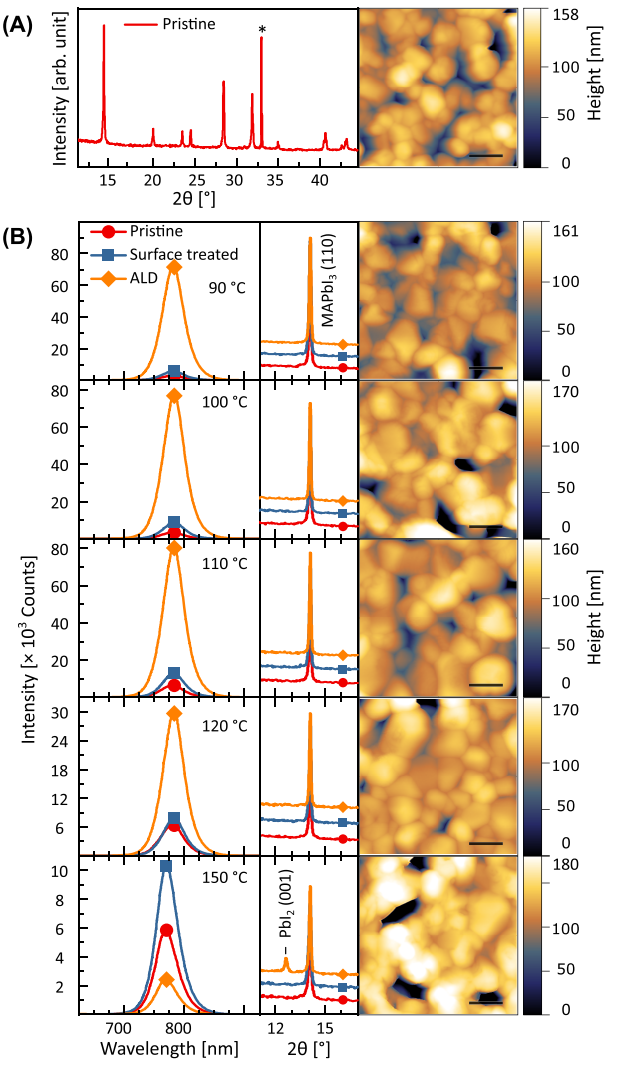

Figure 2. Effects of the ALD processing temperature on the material integrity of the underlying $MAPbI_3$ films. (A) An XRD pattern and an AFM image of a pristine $MAPbI_3$ film on a (100) Si substrate. The peak indicated by an asterisk belongs to the Si substrate. (B) Steady-state PL spectra (left panels) and XRD patterns (middle panels) of pristine (red), surface-treated (blue), and post-ALD (orange) samples. From top to bottom, 100 cycles of thermal ALD were conducted at 90, 100, 110, 120, and 150 °C, respectively. Right panels: the AFM images of the perovskite film on Si substrate after 100 cycles of thermal ALD at the corresponding temperatures. All of the scale bars in the AFM images are 200 nm.

The appearance of PbI_2 was accompanied by changes in optical properties. While photoluminescence (PL) of $MAPbI_3$ increased slightly after the surface treatment, much more pronounced effects on the PL intensity were observed after the ALD procedure. In the temperature range where the integrity of the perovskite layer was preserved, the PL intensity increased after the ALD procedure. This could be attributed to the passivation of the nonradiative defects on the surface of $MAPbI_3$. Such passivation could be facilitated by a small amount of PbI_2 formed on the surface or the interfacial electric field caused by the negative charges in the amorphous Al_2O_3.[44−47] When the substrate temperature was further increased (>120 °C), the PL intensity decreased (Figure 2B, left panels) and PbI_2 started to form (Figure 2B, middle panels). Such a decrease could be related to the formation of crystal defects or changes of chemical composition,[48,49] both of which were undesirable for the best optoelectronic performance in devices. The integrity of the perovskite films was also inspected by topographic mapping using atomic force microscopy (AFM) (Figure 2A,B, right panels). While the surface topography showed minimal changes at lower temperatures (90 and 100 °C), noticeable grain coalescence was observed in $MAPbI_3$ films that experienced ALD processing at higher temperatures (120 and 150 °C). Based on the optical, crystallographic, and morphological characterizations, 90−120 °C was identified as the range of optimal processing temperature. The nondestructive nature of the ALD processing at this temperature was also evident by the retained crystallinity in underlying $MAPbI_3$ layer (Figure 1B, insets).

The efficacy of the ALD processing was further improved when the plasma-enhanced mode was introduced. As opposed to the conventional thermal ALD where water vapor was used as a coreactant, the more recently developed plasma-enhanced ALD completed coating reactions by generating oxygen radicals using an RF plasma generator. Such a different reaction mechanism allowed for better coating quality at moderate temperatures due to the high reactivity of the energetic oxygen radicals with organometal precursors.[31] These advantages made the plasma-enhanced ALD highly favorable for depositing directly on the hybrid perovskites. Unfortunately, bare surfaces of the perovskites were subject to considerable plasma damage. After only 20 cycles of plasma-enhanced ALD conducted at 90 °C, the perovskite exhibited substantial decays in PL intensity, and PbI_2 was detected by using XRD (Figure 3A and Figure S3).

To circumvent the plasma damage, we employed a novel strategy by combining thermal and plasma-enhanced ALD into the deposition of the same layer of Al_2O_3. The thermal ALD preceded the plasma-enhanced ALD to provide a few monolayers of Al_2O_3 for protection purposes. Surprisingly, 10 cycles of thermal ALD (<1 nm Al_2O_3) were sufficient to protect the underlying perovskite against the plasma damage. Neither photoluminescence nor XRD showed signs of degradation of the perovskite after 10 + 90 cycles of hybrid ALD (i.e., 10 cycles of thermal ALD followed by 90 cycles of plasma-enhanced ALD) (Figure 3B). The prior thermal ALD with five cycles was also attempted before the plasma-enhanced ALD; however, the PL showed a decay of intensity (Figure S4).

The improved coating quality obtained by using the hybrid ALD was manifested as much lower permeability against solvents in which the perovskite was known to be soluble. Two $MAPbI_3$ thin films encapsulated by using 10 + 50 cycles of

https://doi.org/10.1021/acs.jpclett.2c00862
J. Phys. Chem. Lett. 2022, 13, 4082−4089

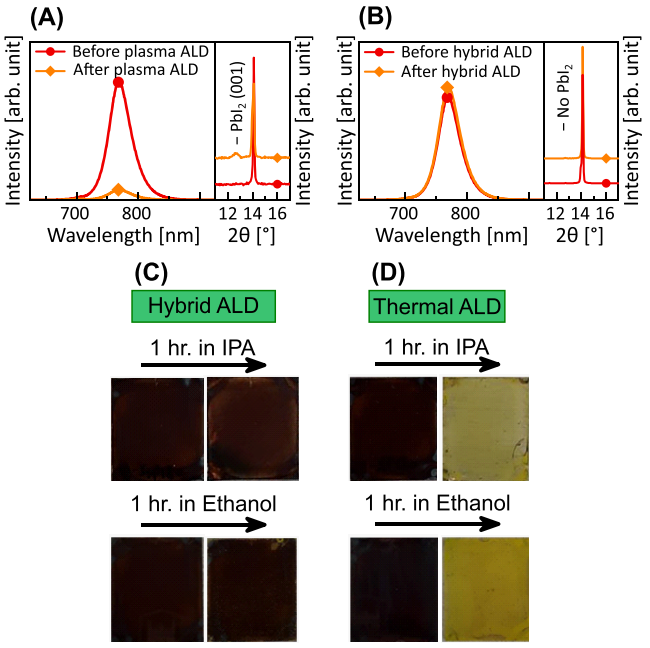

Figure 3. Effects of including plasma-assisted ALD in the final Al_2O_3 film quality and material integrity of $MAPbI_3$ substrate. Steady-state PL spectra (left panel) and XRD patterns (right panel) of surface-treated $MAPbI_3$ before and after (A) 20 cycles of plasma-assisted and (B) 10 + 90 cycles of hybrid ALD at 90 °C. Pictures of $MAPbI_3$ films on glass substrate with (C) 10 + 50 cycles of hybrid ALD at 90 °C and (D) 60 cycles of 90 °C thermal ALD, before and after soaking them in isopropanol and ethanol for 1 h.

hybrid ALD and 60 cycles of thermal ALD were immersed in the solvents (isopropanol and ethanol). The former showed no visible changes after 1 h of immersion whereas the latter was almost completely dissolved (Figure 3C,D). By studying the effects of molecular surface treatment on the ALD Al_2O_3 coating quality, we further unveiled the promoted ALD film robustness in light of the suppressed decomposition of perovskite film (Figure S5). The resistance to strong solvents demonstrated the promise of inhibiting interfacial reactions in perovskite-based devices by using ultrathin ALD interlayers.

What might also be crucial to the successful encapsulation was to assemble selected small molecules on the surface of the perovskite film—a step for preparing the surface for the following ALD. Water was widely used as the coreactant in many established ALD recipes when depositing metal oxides. Often, such ALD procedures began with a pulse of water vapor to prime the substrates with hydroxyl groups, a desirable termination for receiving the subsequent precursor. Hybrid perovskites, however, were known to be soluble in water.[50,51] Besides the possible surface damages, the perovskites would not be properly primed by the water vapor, leading to compromised surface coverage especially during the first few cycles of thermal ALD. To address this problem, we attempted to modify the perovskite surface using 2-mcpEtOH with the expectation that the S in the thiol group would bond with Pb^{2+} of the perovskite due to a stronger coordination.[52] Thin films of perovskites were immersed in 2-mcpEtOH vapor in an evacuated quartz tube with controlled temperature and pressure (more details in the Experimental Methods section).

The presence of the surface assembled molecules was confirmed by using solid-state ^{1}H NMR. The hydroxyl protons (OH) and thiol protons (SH) resonate at around 4.9 ppm (H2) and −0.16 ppm (H5), respectively (Figure 4A). Interestingly, the bonding configuration of 2-mcpEtOH on the surface of $MAPbI_3$ turned out to be quite different from our expectation. The integrated areas under the corresponding NMR peaks inferred a greater amount of SH than OH (7.18:2.55) in the molecules attached to the surface (Figure 4A,C and Table S1), suggesting that the perovskite surface was

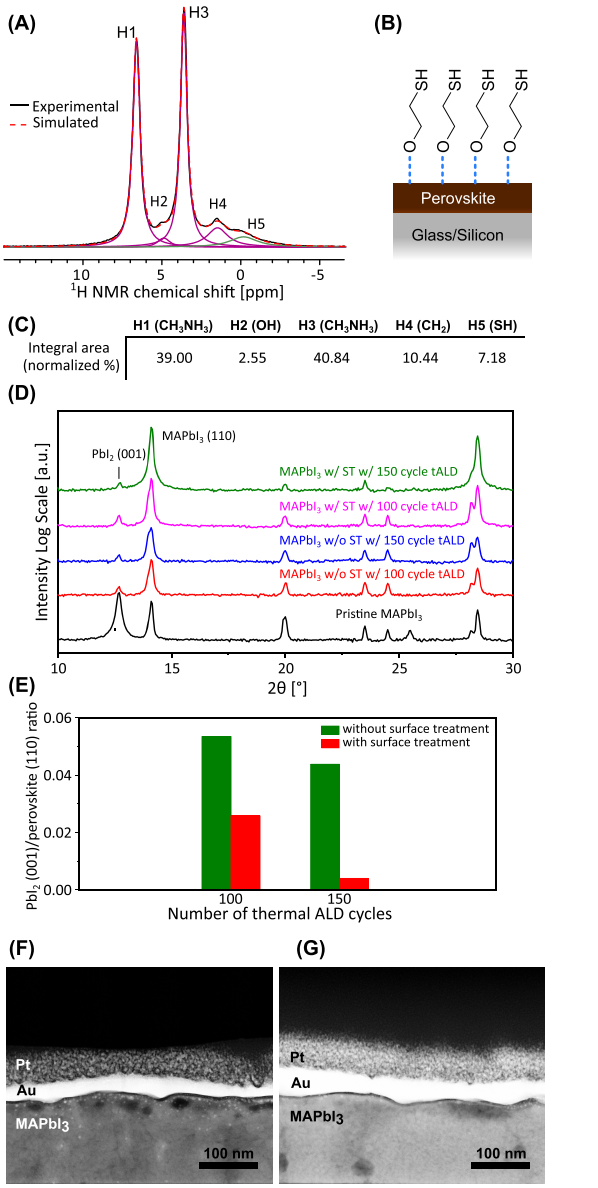

Figure 4. Effects of 2-mcpEtOH in the growth efficacy of ALD-Al_2O_3. (A) Solid-state ^{1}H NMR spectrum of 2-mcpEtOH-treated $MAPbI_3$ powder as scraped from thin films. (B) Schematic illustration of 2-mcpEtOH adsorption on $MAPbI_3$. (C) Summary of proton compositions from different functional groups as extracted from the peak fittings in (A). (D) XRD of ALD-coated and uncoated perovskites after exposing to in saturated water vapor at 1 atm for 40 h. The PbI_2 (001) peak around 12.5° can be viewed as an indication of water-induced decomposition of the perovskite. (E) Comparison of the integrated areas under the PbI_2 (001) peak showed that the water-induced decomposition was much more severe without the surface molecular treatment. Cross-section TEM images of 10 + 20 cycles of hybrid ALD Al_2O_3-coated $MAPbI_3$ (F) with and (G) without the surface treatment.

https://doi.org/10.1021/acs.jpclett.2c00862
J. Phys. Chem. Lett. 2022, 13, 4082−4089

primarily thiolated instead of hydroxylated after the molecular modification (Figure 4B).

Despite the unexpected bonding scheme, the surface treatment led to desirable outcomes in the subsequent ALD processing. After being exposed to saturated water for 40 h (Figure S6), perovskites coated with the Al_2O_3 layer, regardless of being molecularly treated or not, exhibited substantially stronger chemical resistance compared to a bare, unprotected perovskite thin film (Figure 4D). The PbI_2 (001) peak around 12.5° in the XRD patterns could be viewed as an indication of the water-induced decomposition. A closer look at the XRD patterns showed that the under-the-curve areas of the PbI_2 (001) peak were much smaller in the samples being treated by 2-mcpEtOH treatment prior to ALD (Figure 4E). The difference in the chemical resistance could also be visualized by the appearance and the color of the samples immersed in water (Figure S7). It is worth noting that minimal difference, between the molecularly treated or untreated samples, could not be captured in the morphology of the subsequent ALD coatings (Figure 4F,G). We speculate that the permeable channels in the amorphous Al_2O_3 must be extremely microscopic, beyond the spatial resolution of a high-resolution TEM. The morphology, even if imaged by using the STEM mode, could not be used to evaluate the quality of the ALD encapsulation as well as the resulted chemical protection. For clarifications, the 2-mcpEtOH molecules themselves, without the ALD coating, did not provide obvious protection to the perovskite films (Figure S8).

In summary, we established a protocol to grow a high-quality, pinhole-free, thin layer of Al_2O_3 film directly on $MAPbI_3$ using ALD. We were able to control the processing conditions so that the ALD processing did not degrade the underlying perovskite chemically, morphologically, or optically. The success could be largely attributed to modifying the surface of perovskite by 2-mcpEtOH and incorporating the plasma-assisted ALD with the conventional thermal mode. Significant improvement in the chemical resistance against environmental stresses was observed with the ALD encapsulation. While the remarkable chemical protection from the ALD encapsulation was demonstrated by using ~7 nm Al_2O_3 interlayers, the thickness may be further reduced in solid-state devices. Interdiffusion between solid materials (i.e., the perovskite and charge transport layers) may be different from the behavior we observed in the solvent soaking experiments reported here. Previous works had shown that >20 cycles of Al_2O_3 ALD can increase the electrical impedance of a photovoltaic device considerably.[21] We found that 10 + 5 cycles of hybrid ALD could still provide considerable chemical protection to the perovskite layer compared to an unprotected one (Figure S9). Future work will need to be focused on the effect of the ALD interlayer on inhibiting interfacial ion exchange in more realistic perovskite-based devices.

The success with the Al_2O_3, the model material used in this work, showed implications on other compounds to be coated on hybrid perovskites using ALD. The alternative coating materials such as SnO_2 or TiO_2 could come with more desirable electrical properties, which can be further multifunctional if used as an interlayer between the perovskite and the transport layers, or electrodes, in devices. Our findings intrigued questions regarding the effects of the ALD layer and its growth conditions on both electrical and optical properties of the perovskite layer. Further studies, therefore, are needed to understand processing−property correlations and establish ALD coating as a standard method for encapsulating hybrid perovskites.

EXPERIMENTAL METHODS

Chemicals, ALD Precursors, and Gases. CH_3NH_3I (MAI, ≥99.99%) was purchased from Greatcell Solar Materials. Lead iodide (PbI_2, 99%), diethyl ether (≥99.0%), γ-butyrolactone (GBL, ≥99%), and 2-mercaptoethanol (2-mcpEtOH, ≥99.0%) were purchased from Aldrich. Trimethylaluminum (TMA, ≥98%, prepackaged in 50 mL Swagelok cylinder) and ultrahigh purity water (H_2O, 99.999%, prepackaged in 50 mL Swagelok cylinder) were purchased from Strem Chemicals. Acetone (≥99.5%) and isopropanol (≥99.5%) were purchased from BDH VWR Analytical. Argon (Ar, ultrahigh purity grade, 300 cf cylinder) and oxygen (O_2, research grade, 300 CF cylinder) were purchased from Airgas. All chemicals were used as received without further purification.

$MAPbI_3$ Perovskite Film Synthesis. A 1:1.05 molar ratio of PbI_2/MAI was first dissolved in GBL with stirring and heating at 40 °C to make a 1 M solution. Glass and P-doped silicon wafers were sequentially sonicated in Alconox (1% aqueous detergent solution), deionized water, acetone, and isopropanol for 15 min in each step. The precursor solution then was spin-coated in an ambient environment on cleaned glass substrates and P-doped silicon wafers by a two-step protocol. Substrates first spun at 200 rpm for 10 s with an 85 rpm s^{-1} ramping rate followed by 3000 rpm for 20 s with the acceleration 340 rpm s^{-1}. The wet films, afterward, were soaked in a diethyl ether bath (~20 mL) for crystallization for ~30 s. The as-synthesized perovskite films were then thermally annealed at 100 °C on a hot plate in a N_2 glovebox for 10 min. The perovskite films on silicon and glass substrates were routinely prepared at the same time. The composition, crystallinity, and morphology of the perovskite thin films were characterized and compared to ensure negligible differences in the synthetic product obtained between the two types of substrates.

2-mcpEtOH Surface Treatment. $MAPbI_3$ films were surface treated with 2-mcpEtOH vapor in a quartz tube of a tube furnace (Thermo Scientific, Lindberg Blue M). $MAPbI_3$ films were placed at the center heating area of the quartz tube, sitting on a glass slide. 50 μL of 2-mcpEtOH in an alumina boat was then placed at the cold side of the furnace, away from the heating coil. The tube was pumped through a mass flow controller (Alicat Scientific) with a 30 Torr pressure set point. The target temperature was set at 80 °C, at which surface treatment continued for 30 min before the furnace heating was turned off. The $MAPbI_3$ film were removed after cooling to below 50 °C under vacuum.

Atomic Layer Deposition (ALD). ALD Al_2O_3 was deposited with a Fiji G2 system. The reactor chamber was first heated to the designated ALD growth temperatures and allowed to stabilize for 15 min. $MAPbI_3$ films with and without 2-mcpEtOH surface treatment were first placed in the load lock and pumped below 2×10^{-5} Torr before being transferred into the reactor. Before the beginning of ALD growth cycles, carrier Ar and plasma Ar gas were flown through delivery line and ALD reactor at 30 and 80 sccm for 20 s, respectively. Each thermal ALD cycle consisted of a TMA pulse of 0.06 s, an Ar purge of 5.2 s, a H_2O pulse of 0.06 s, and then a purge time of 10 s. On the other hand, each plasma ALD cycle was constituted of a TMA pulse of 0.06 s, an Ar purge of 5.2 s, and

https://doi.org/10.1021/acs.jpclett.2c00862
J. Phys. Chem. Lett. 2022, 13, 4082−4089

then a 300 W oxygen plasma of 6 s followed by a purge time of 4 s. During the ALD processes, the delivery line and valve manifold of the system were kept at 150 °C. No pre- and postdeposition thermal annealing of the $MAPbI_3$ films were performed. During the ALD processing, the surface of the perovskite is acting as the actual receiving substrate. Therefore, we do not expect, nor did we observe, substantial effects from the Si or glass on Al_2O_3 coating.

Solid-State ^{1}H NMR. A high-resolution ^{1}H NMR spectrum of $MAPbI_3$ was collected on a Bruker 600 MHz spectrometer. The samples were packed into 1.3 mm NMR rotors in an argon-filled glovebox. A rotor-synchronized spin-echo pulse sequence with a $\pi/2$ pulse length of 2.9 μs was used to acquire the spectrum. The magic angle spinning (MAS) rate was 50 kHz. The NMR spectra were calibrated by using adamantane at 1.83 ppm.

■ ASSOCIATED CONTENT

Supporting Information

The Supporting Information is available free of charge at https://pubs.acs.org/doi/10.1021/acs.jpclett.2c00862.

Additional experimental details include plane-view EDS spectrum, cross-section elemental mapping of ALD-coated $MAPbI_3$ films, ^{1}H solid-state NMR peak information, PL spectrum and XRD pattern of perovskite films without surface treatment, PL spectra of perovskite films before and after hybrid ALD, photographs of 100 cycles thermal ALD-coated perovskite films soaked in isopropanol, photographs of water vapor aging setup, photographs of perovskite films soaked in water, photographs and *in situ* PL peak intensity of surface-treated perovskite films soaked in ethanol, photographs of perovskite films with hybrid ALD soaked in isopropanol, photographs and *in situ* PL peak intensity of a pristine perovskite film soaked in isopropanol (PDF)

■ AUTHOR INFORMATION

Corresponding Author

Hanwei Gao − *Department of Physics and Materials Science and Engineering Program, Florida State University, Tallahassee, Florida 32306, United States; Condensed Matter Science, National High Magnetic Field Laboratory, Tallahassee, Florida 32310, United States;* orcid.org/0000-0001-8085-8178; Email: hanwei.gao@fsu.edu

Authors

Jue Gong − *Department of Physics, Florida State University, Tallahassee, Florida 32306, United States;* orcid.org/0000-0001-8089-5796

Moein Adnani − *Department of Physics, Florida State University, Tallahassee, Florida 32306, United States;* orcid.org/0000-0001-8115-1414

Brendon T. Jones − *Department of Physics, Florida State University, Tallahassee, Florida 32306, United States*

Yan Xin − *Condensed Matter Science, National High Magnetic Field Laboratory, Tallahassee, Florida 32310, United States*

Sisi Wang − *Department of Chemistry and Biochemistry, Florida State University, Tallahassee, Florida 32306, United States*

Sawankumar V. Patel − *Department of Chemistry and Biochemistry, Florida State University, Tallahassee, Florida 32306, United States;* orcid.org/0000-0002-5293-9330

Eric Lochner − *Department of Physics, Florida State University, Tallahassee, Florida 32306, United States*

Hedi Mattoussi − *Department of Chemistry and Biochemistry, Florida State University, Tallahassee, Florida 32306, United States;* orcid.org/0000-0002-6511-9323

Yan-Yan Hu − *Department of Chemistry and Biochemistry and Materials Science and Engineering Program, Florida State University, Tallahassee, Florida 32306, United States;* orcid.org/0000-0003-0677-5897

Complete contact information is available at: https://pubs.acs.org/10.1021/acs.jpclett.2c00862

Notes

The authors declare no competing financial interest.

■ ACKNOWLEDGMENTS

The authors thank Prof. Lea Nienhaus and Mr. Benjamin Chen for insightful discussions. The work was supported by National Science Foundation (ECCS-2131610). The atomic layer deposition was performed by using an instrument acquired with funding from National Science Foundation (MRI-1828090). H.G. acknowledges the support from the Office of Naval Research (N00014-18-1-2408). S.V.P. and Y.-Y.H. acknowledge the support from National Science Foundation (DMR-1847038). S.W. and H.M. acknowledge the support from National Science Foundation (CHE-2005079). This work used equipment in the FSU Physics Department CMMP User Facility and the Chemistry Department MAC Laboratory. The solid-state NMR and electron microscopy measurements were performed at the National High Magnetic Field Laboratory, which is supported by National Science Foundation Cooperative Agreement No. DMR-1644779 and the State of Florida.

■ REFERENCES

(1) Min, H.; Lee, D. Y.; Kim, J.; Kim, G.; Lee, K. S.; Kim, J.; Paik, M. J.; Kim, Y. K.; Kim, K. S.; Kim, M. G.; Shin, T. J.; Seok, S. I. Perovskite Solar Cells with Atomically Coherent Interlayers on SnO_2 Electrodes. *Nature* **2021**, *598*, 444−450.

(2) Tong, J.; Gong, J.; Hu, M.; Yadavalli, S. K.; Dai, Z.; Zhang, F.; Xiao, C.; Hao, J.; Yang, M.; Anderson, M. A.; Ratcliff, E. L.; Berry, J. J.; Padture, N. P.; Zhou, Y.; Zhu, K. High-performance methylammonium-free ideal-band-gap perovskite solar cells. *Matter* **2021**, *4*, 1365−1376.

(3) Zhao, J.; Zhao, L.; Deng, Y.; Xiao, X.; Ni, Z.; Xu, S.; Huang, J. Perovskite-filled membranes for flexible and large-area direct-conversion X-ray detector arrays. *Nat. Photonics* **2020**, *14*, 612−617.

(4) He, Y.; Petryk, M.; Liu, Z.; Chica, D. G.; Hadar, I.; Leak, C.; Ke, W.; Spanopoulos, I.; Lin, W.; Chung, D. Y.; Wessels, B. W.; He, Z.; Kanatzidis, M. G. $CsPbBr_3$ perovskite detectors with 1.4% energy resolution for high-energy γ-rays. *Nat. Photonics* **2021**, *15*, 36−42.

(5) Zhu, H.; Fu, Y.; Meng, F.; Wu, X.; Gong, Z.; Ding, Q.; Gustafsson, M. V.; Trinh, M. T.; Jin, S.; Zhu, X.-Y. Lead halide perovskite nanowire lasers with low lasing thresholds and high quality factors. *Nat. Mater.* **2015**, *14*, 636−642.

(6) Fu, Y.; Zhu, H.; Schrader, A. W.; Liang, D.; Ding, Q.; Joshi, P.; Hwang, L.; Zhu, X.-Y.; Jin, S. Nanowire Lasers of Formamidinium Lead Halide Perovskites and Their Stabilized Alloys with Improved Stability. *Nano Lett.* **2016**, *16*, 1000−1008.

(7) Yin, W.-J.; Shi, T.; Yan, Y. Unique Properties of Halide Perovskites as Possible Origins of the Superior Solar Cell Performance. *Adv. Mater.* **2014**, *26*, 4653−4658.

(8) Kazim, S.; Nazeeruddin, M. K.; Grätzel, M.; Ahmad, S. Perovskite as Light Harvester: A Game Changer in Photovoltaics. *Angew. Chem., Int. Ed.* **2014**, *53*, 2812−2824.
(9) Shi, D.; Adinolfi, V.; Comin, R.; Yuan, M.; Alarousu, E.; Buin, A.; Chen, Y.; Hoogland, S.; Rothenberger, A.; Katsiev, K.; Losovyj, Y.; Zhang, X.; Dowben, P. A.; Mohammed, O. F.; Sargent, E. H.; Bakr, O. M. Low trap-state density and long carrier diffusion in organolead trihalide perovskite single crystals. *Science* **2015**, *347*, 519−522.
(10) Stranks, S. D.; Eperon, G. E.; Grancini, G.; Menelaou, C.; Alcocer, M. J. P.; Leijtens, T.; Herz, L. M.; Petrozza, A.; Snaith, H. J. Electron-Hole Diffusion Lengths Exceeding 1 Micrometer in an Organometal Trihalide Perovskite Absorber. *Science* **2013**, *342*, 341−344.
(11) Yuan, Y.; Wang, Q.; Shao, Y.; Lu, H.; Li, T.; Gruverman, A.; Huang, J. Electric-Field-Driven Reversible Conversion Between Methylammonium Lead Triiodide Perovskites and Lead Iodide at Elevated Temperatures. *Adv. Energy Mater.* **2016**, *6*, 1501803.
(12) Howard, J. M.; Tennyson, E. M.; Barik, S.; Szostak, R.; Waks, E.; Toney, M. F.; Nogueira, A. F.; Neves, B. R. A.; Leite, M. S. Humidity-Induced Photoluminescence Hysteresis in Variable Cs/Br Ratio Hybrid Perovskites. *J. Phys. Chem. Lett.* **2018**, *9*, 3463−3469.
(13) Tong, C. J.; Geng, W.; Prezhdo, O. V.; Liu, L. M. Role of Methylammonium Orientation in Ion Diffusion and Current-Voltage Hysteresis in the $CH_3NH_3PbI_3$ Perovskite. *ACS Energy Lett.* **2017**, *2*, 1997−2004.
(14) Wei, J.; Wang, Q.; Huo, J.; Gao, F.; Gan, Z.; Zhao, Q.; Li, H. Mechanisms and Suppression of Photoinduced Degradation in Perovskite Solar Cells. *Adv. Energy Mater.* **2021**, *11*, 2002326.
(15) Di Girolamo, D.; Phung, N.; Kosasih, F. U.; Di Giacomo, F.; Matteocci, F.; Smith, J. A.; Flatken, M. A.; Kobler, H.; Turren Cruz, S. H.; Mattoni, A.; Cina, L.; Rech, B.; Latini, A.; Divitini, G.; Ducati, C.; Di Carlo, A.; Dini, D.; Abate, A. Ion Migration-Induced Amorphization and Phase Segregation as a Degradation Mechanism in Planar Perovskite Solar Cells. *Adv. Energy Mater.* **2020**, *10*, 2000310.
(16) Cheng, T.; Tumen-Ulzii, G.; Klotz, D.; Watanabe, S.; Matsushima, T.; Adachi, C. Ion Migration-Induced Degradation and Efficiency Roll-off in Quasi-2D Perovskite Light-Emitting Diodes. *ACS Appl. Mater. Interfaces* **2020**, *12*, 33004−33013.
(17) Gong, J.; Yang, M.; Rebollar, D.; Rucinski, J.; Liveris, Z.; Zhu, K.; Xu, T. Divalent Anionic Doping in Perovskite Solar Cells for Enhanced Chemical Stability. *Adv. Mater.* **2018**, *30*, 1800973.
(18) Huang, Z.; Proppe, A. H.; Tan, H.; Saidaminov, M. I.; Tan, F.; Mei, A.; Tan, C.-S.; Wei, M.; Hou, Y.; Han, H.; Kelley, S. O.; Sargent, E. H. Suppressed Ion Migration in Reduced-Dimensional Perovskites Improves Operating Stability. *ACS Energy Lett.* **2019**, *4*, 1521−1527.
(19) Ma, Y.; Cheng, Y.; Xu, X.; Li, M.; Zhang, C.; Cheung, S. H.; Zeng, Z.; Shen, D.; Xie, Y.-M.; Chiu, K. L.; Lin, F.; So, S. K.; Lee, C.-S.; Tsang, S.-W. Suppressing Ion Migration across Perovskite Grain Boundaries by Polymer Additives. *Adv. Funct. Mater.* **2021**, *31*, 2006802.
(20) George, S. M. Atomic Layer Deposition: An Overview. *Chem. Rev.* **2010**, *110*, 111−131.
(21) Koushik, D.; Verhees, W. J. H.; Kuang, Y.; Veenstra, S.; Zhang, D.; Verheijen, M. A.; Creatore, M.; Schropp, R. E. I. High-dfficiency humidity-stable planar perovskite solar cells based on atomic layer architecture. *Energy Environ. Sci.* **2017**, *10*, 91−100.
(22) Das, C.; Kot, M.; Hellmann, T.; Wittich, C.; Mankel, E.; Zimmermann, I.; Schmeisser, D.; Khaja Nazeeruddin, M.; Jaegermann, W. Atomic Layer-Deposited Aluminum Oxide Hinders Iodide Migration and Stabilizes Perovskite Solar Cells. *Cell Rep. Phys. Sci.* **2020**, *1*, 100112.
(23) Brinkmann, K. O.; Gahlmann, T.; Riedl, T. Atomic Layer Deposition of Functional Layers in Planar Perovskite Solar Cells. *Sol. RRL* **2020**, *4*, 1900332.
(24) Kot, M.; Kegelmann, L.; Das, C.; Kus, P.; Tsud, N.; Matolinova, I.; Albrecht, S.; Matolin, V.; Schmeisser, D. Room-Temperature Atomic-Layer-Deposited Al_2O_3 Improves the Efficiency of Perovskite Solar Cells over Time. *ChemSusChem* **2018**, *11*, 3640−3648.
(25) Seo, S.; Jeong, S.; Park, H.; Shin, H.; Park, N.-G. Atomic layer deposition for efficient and stable perovskite solar cells. *Chem. Commun.* **2019**, *55*, 2403−2416.
(26) Kim, I. S.; Martinson, A. B. F. Stabilizing hybrid perovskites against moisture and temperature *via* non-hydrolytic atomic layer deposited overlayers. *J. Mater. Chem. A* **2015**, *3*, 20092−20096.
(27) Hultqvist, A.; Aitola, K.; Sveinbjörnsson, K.; Saki, Z.; Larsson, F.; Törndahl, T.; Johansson, E.; Boschloo, G.; Edoff, M. Atomic Layer Deposition of Electron Selective SnOx and ZnO Films on Mixed Halide Perovskite: Compatibility and Performance. *ACS Appl. Mater. Interfaces* **2017**, *9*, 29707−29716.
(28) Palmstrom, A. F.; Raiford, J. A.; Prasanna, R.; Bush, K. A.; Sponseller, M.; Cheacharoen, R.; Minichetti, M. C.; Bergsman, D. S.; Leijtens, T.; Wang, H.-P.; Bulović, V.; McGehee, M. D.; Bent, S. F. Interfacial Effects of Tin Oxide Atomic Layer Deposition in Metal Halide Perovskite Photovoltaics. *Adv. Energy Mater.* **2018**, *8*, 1800591.
(29) Hultqvist, A.; Jacobsson, T. J.; Svanström, S.; Edoff, M.; Cappel, U. B.; Rensmo, H.; Johansson, E. M. J.; Boschloo, G.; Törndahl, T. SnOx Atomic Layer Deposition on Bare Perovskite - An Investigation of Initial Growth Dynamics, Interface Chemistry, and Solar Cell Performance. *ACS Appl. Energy Mater.* **2021**, *4*, 510−522.
(30) Jena, A. K.; Kulkarni, A.; Miyasaka, T. Halide Perovskite Photovoltaics: Background, Status, and Future Prospects. *Chem. Rev.* **2019**, *119*, 3036−3103.
(31) Oviroh, P. O.; Akbarzadeh, R.; Pan, D.; Coetzee, R. A. M.; Jen, T.-C. New development of atomic layer deposition: processes, methods and applications. *Sci. Technol. Adv. Mater.* **2019**, *20*, 465−496.
(32) Groner, M. D.; Fabreguette, F. H.; Elam, J. W.; George, S. M. Low-Temperature Al_2O_3 Atomic Layer Deposition. *Chem. Mater.* **2004**, *16*, 639−645.
(33) Park, J. H.; Fathipour, S.; Kwak, I.; Sardashti, K.; Ahles, C. F.; Wolf, S. F.; Edmonds, M.; Vishwanath, S.; Xing, H. G.; Fullerton-Shirey, S. K.; Seabaugh, A.; Kummel, A. C. Atomic Layer Deposition of Al_2O_3 on WSe_2 Functionalized by Titanyl Phthalocyanine. *ACS Nano* **2016**, *10*, 6888−6896.
(34) Etinger-Geller, Y.; Polishchuk, I.; Seknazi, E.; Livne, A.; Ciatto, G.; Pokroy, B. Surface reconstruction causes structural variations in nanometric amorphous Al_2O_3. *Phys. Chem. Chem. Phys.* **2019**, *21*, 14887−14891.
(35) Etinger-Geller, Y.; Zoubenko, E.; Baskin, M.; Kornblum, L.; Pokroy, B. Thickness dependence of the physical properties of atomic-layer deposited Al_2O_3. *J. Appl. Phys.* **2019**, *125*, 185302.
(36) Ma, L.; Guo, D.; Li, M.; Wang, C.; Zhou, Z.; Zhao, X.; Zhang, F.; Ao, Z.; Nie, Z. Temperature-Dependent Thermal Decomposition Pathway of Organic-Inorganic Halide Perovskite Materials. *Chem. Mater.* **2019**, *31*, 8515−8522.
(37) Dualeh, A.; Gao, P.; Seok, S. I.; Nazeeruddin, M. K.; Grätzel, M. Thermal Behavior of Methylammonium Lead-Trihalide Perovskite Photovoltaic Light Harvesters. *Chem. Mater.* **2014**, *26*, 6160−6164.
(38) Hiraiwa, A.; Saito, T.; Matsumura, D.; Kawarada, H. Isotope analysis of diamond-surface passivation effect of high-temperature H_2O-grown atomic layer deposition-Al_2O_3 films. *J. Appl. Phys.* **2015**, *117*, 215304.
(39) van Hemmen, J. L.; Heil, S. B. S.; Klootwijk, J. H.; Roozeboom, F.; Hodson, C. J.; van de Sanden, M. C. M.; Kessels, W. M. M. Plasma and Thermal ALD of Al_2O_3 in a Commercial 200 mm ALD Reactor. *J. Electrochem. Soc.* **2007**, *154*, G165.
(40) Johnson, R. W.; Hultqvist, A.; Bent, S. F. A brief review of atomic layer deposition: from fundamentals to applications. *Mater. Today* **2014**, *17*, 236−246.
(41) Kim, N.-K.; Min, Y. H.; Noh, S.; Cho, E.; Jeong, G.; Joo, M.; Ahn, S.-W.; Lee, J. S.; Kim, S.; Ihm, K.; Ahn, H.; Kang, Y.; Lee, H.-S.; Kim, D. Investigation of Thermally Induced Degradation in $CH_3NH_3PbI_3$ Perovskite Solar Cells using *In-Situ* Synchrotron Radiation Analysis. *Sci. Rep.* **2017**, *7*, 4645.

https://doi.org/10.1021/acs.jpclett.2c00862
J. Phys. Chem. Lett. 2022, 13, 4082−4089

(42) Gong, J.; Guo, P.; Benjamin, S. E.; Van Patten, P. G.; Schaller, R. D.; Xu, T. Cation engineering on lead iodide perovskites for stable and high-performance photovoltaic applications. *J. Energy Chem.* **2018**, *27*, 1017−1039.
(43) Juarez-Perez, E. J.; Hawash, Z.; Raga, S. R.; Ono, L. K.; Qi, Y. Thermal degradation of $CH_3NH_3PbI_3$ perovskite into NH_3 and CH_3I gases observed by coupled thermogravimetry-mass spectrometry analysis. *Energy Environ. Sci.* **2016**, *9*, 3406−3410.
(44) Shi, B.; Yao, X.; Hou, F.; Guo, S.; Li, Y.; Wei, C.; Ding, Y.; Li, Y.; Zhao, Y.; Zhang, X. Unraveling the Passivation Process of PbI_2 to Enhance the Efficiency of Planar Perovskite Solar Cells. *J. Phys. Chem. C* **2018**, *122*, 21269−21276.
(45) Cook, A.; Jones, T. W.; Wang, J. T.-W.; Li, H.; Atkin, R.; Duffy, N. W.; Donne, S. W.; Wilson, G. J. Passivation by pyridine-induced PbI_2 in methylammonium lead iodide perovskites. *RSC Adv.* **2020**, *10*, 23829−23833.
(46) Bonilla, R. S.; Hoex, B.; Hamer, P.; Wilshaw, P. R. Dielectric surface passivation for silicon solar cells: A review. *Phys. Status Solidi Appl. Mater. Sci.* **2017**, *214*, 1700293.
(47) Dingemans, G.; Kessels, W. M. M. Status and prospects of Al_2O_3-based surface passivation schemes for silicon solar cells. *J. Vac. Sci. Technol.* **2012**, *30*, 040802.
(48) Kong, L.; Gong, J.; Hu, Q.; Capitani, F.; Celeste, A.; Hattori, T.; Sano-Furukawa, A.; Li, N.; Yang, W.; Liu, G.; Mao, H.-k. Suppressed Lattice Disorder for Large Emission Enhancement and Structural Robustness in Hybrid Lead Iodide Perovskite Discovered by High-Pressure Isotope Effect. *Adv. Funct. Mater.* **2021**, *31*, 2009131.
(49) Chen, Y.; Lei, Y.; Li, Y.; Yu, Y.; Cai, J.; Chiu, M.-H.; Rao, R.; Gu, Y.; Wang, C.; Choi, W.; Hu, H.; Wang, C.; Li, Y.; Song, J.; Zhang, J.; Qi, B.; Lin, M.; Zhang, Z.; Islam, A. E.; Maruyama, B.; Dayeh, S.; Li, L.-J.; Yang, K.; Lo, Y.-H.; Xu, S. Strain engineering and epitaxial stabilization of halide perovskites. *Nature* **2020**, *577*, 209−215.
(50) Kim, B. J.; Kim, D. H.; Kwon, S. L.; Park, S. Y.; Li, Z.; Zhu, K.; Jung, H. S. Selective dissolution of halide perovskites as a step towards recycling solar cells. *Nat. Commun.* **2016**, *7*, 11735.
(51) Leguy, A. M. A.; Hu, Y.; Campoy-Quiles, M.; Alonso, M. I.; Weber, O. J.; Azarhoosh, P.; van Schilfgaarde, M.; Weller, M. T.; Bein, T.; Nelson, J.; Docampo, P.; Barnes, P. R. F. Reversible Hydration of $CH_3NH_3PbI_3$ in Films, Single Crystals, and Solar Cells. *Chem. Mater.* **2015**, *27*, 3397−3407.
(52) Hamill, J. C., Jr.; Romiluyi, O.; Thomas, S. A.; Cetola, J.; Schwartz, J.; Toney, M. F.; Clancy, P.; Loo, Y.-L. Sulfur-Donor Solvents Strongly Coordinate Pb^{2+} in Hybrid Organic-Inorganic Perovskite Precursor Solutions. *J. Phys. Chem. C* **2020**, *124*, 14496−14502.

https://doi.org/10.1021/acs.jpclett.2c00862
J. Phys. Chem. Lett. 2022, 13, 4082−4089